CrystEngComm

ROYAL SOCIETY OF CHEMISTRY

COMMUNICATION

View Article Online
View Journal | View Issue

Check for updates

Cite this: *CrystEngComm*, 2024, **26**, 2228

Received 7th March 2024,
Accepted 11th March 2024

DOI: 10.1039/d4ce00221k

rsc.li/crystengcomm

Orthogonal stimulation of structural transformations in photo-responsive MOF films through linker functionalization†

Sumea Klokic,[ab] Benedetta Marmiroli,[b] Denys Naumenko,[b] Giovanni Birarda,[c] Simone Dal Zilio,[d] Miriam de J. Velásquez-Hernández,[e] Paolo Falcaro,[e] Lisa Vaccari[c] and Heinz Amenitsch*[b]

Controlling the magnitude of structural dynamics in flexible MOF films by an applied stimulus is largely desired for specific applications such as energy storage. Herein, by introducing chlorine substituents in an azobenzene-infiltrated Cl-DMOF-1 film structure, a significantly slowed structural response is obtained upon photo-switching of the system.

To date, the fabrication of structurally responsive MOF films[1,2] is encouraged for the development of MOF-based devices, including sensors,[3,4] cargo delivery systems[5–7] and mechanical storage systems.[8–10] Implementing a moiety within a film assembly that is responsive to an external stimulus allows for the remote control of MOF film properties.[11] Here, light is a particularly attractive stimulus as it is readily available and renewable in the form of sunlight.[12] So far, a large number of structurally flexible photo-active MOFs has been reported, such as DMOF-1 ($[Zn_2(bdc)_2(dabco)]$, bdc = 1,4-benzenedicarboxylate and dabco = 1,4-diazabicyclo[2.2.2]octan),[13] or $[Zn(AzDC)(4,4'\text{-BPE})_{0.5}]$, AzDC = azobenzene-4,4′-dicarboxylic acid and 4,4′-BPE = *trans*-1,2-bis(4-pyridyl)ethylene.[14] Most of these flexible structures are based on reticular design strategies, where molecular building blocks are replaced within the MOF system.[15,16] These structures exhibit a tuned flexibility that provides an extra degree of freedom, which offers additional means to exploit dynamics in responsive MOF film systems alongside primary photon stimulation. This concept is introduced as orthogonal stimulation by Peh *et al.*[15] and holds promise for tailoring responsiveness in flexible MOF systems. Following this approach, in this study, we demonstrate a chemical pathway to tune photo-induced structural transformations.[15] Replacing terephthalic acid linkers with chloro-functionalized derivatives allows for the fabrication of **Cl-DMOF-1** films that are isostructural to the DMOF-1 system (Fig. 1a, right)[13,17] while exhibiting varied flexibility with changes in growth time (Fig. 1b). Although linker functionalization has been successfully shown for bulk DMOF-1 systems,[18–21] structural photo-response and its duration for such modified structures has not been examined so far. We tackled this by incorporating azobenzene within **Cl-DMOF-1** pores to obtain a photo-responsive film system, which was confirmed by infrared spectroscopic measurements. Time-resolved grazing incidence wide angle X-ray scattering measurements (GIWAXS) showed a

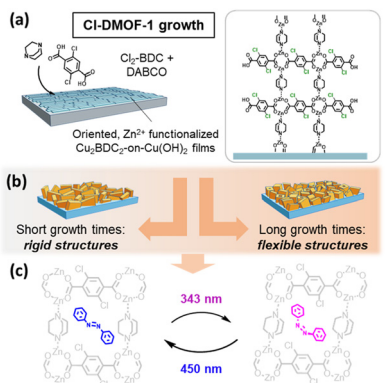

Fig. 1 Schematics of the orthogonal stimulation strategy in MOF films. (a) Structure of the flexible **Cl-DMOF-1** framework viewed along the zinc paddlewheel units linked by functionalized Cl_2-bdc and pillared by dabco. (b) Varying the growth time of the **Cl-DMOF-1** films leads to rigid or flexible structures. (c) **Cl-DMOF-1** films were infiltrated by azobenzene, which upon irradiation with UV light (343 nm) isomerizes from *trans* to *cis* and *vice versa* upon irradiation with blue light (450 nm).

[a] *CERIC-ERIC, Elettra Sincrotrone Trieste – SAXS Beamline, S.S. 14, 163.5 km, Basovizza, Trieste 34149, Italy*
[b] *Institute of Inorganic Chemistry, Graz University of Technology, 8010 Graz, Austria. E-mail: heinz.amentisch@tugraz.at*
[c] *Elettra Sincrotrone Trieste – SISSI Bio Beamline, S.S. 14, 163.5 km, Basovizza, Trieste 34149, Italy*
[d] *IOM-CNR, Laboratorio TASC, S.S. 14, 163.5 km, Basovizza, Trieste 34149, Italy*
[e] *Institute of Physical and Theoretical Chemistry, Graz University of Technology, 8010 Graz, Austria*

† Electronic supplementary information (ESI) available. See DOI: https://doi.org/10.1039/d4ce00221k

significantly slowed structural photo-response compared to the DMOF-1 structure (Fig. 1c).[22]

To ensure sufficient light penetration accompanied by a controlled propagation of structural photo-response, **Cl-DMOF-1** films were fabricated as heteroepitaxial film structures following a substrate-seeded approach.[23,24] For this, in the first step, $Cu(OH)_2$ nanobelts were deposited on glass substrates, which were then converted to Cu_2bdc_2 (see Scheme S1†).[23]

Subsequently, the Cu_2bdc_2-on-$Cu(OH)_2$ films were treated in zinc acetate and placed at 60 °C in the methanolic linker solution containing dabco and a Cl_2-bdc linker (Fig. 1a, see ESI† for experimental details). However, linker functionalization in MOFs can potentially vary the thermodynamic stability and, thus, the readiness of the structure to grow.[25] To address this issue, in the first step, we altered the growth time of the **Cl-DMOF-1** films from 10 to 270 min and studied the alignment of the structure along the Cu_2bdc_2-on-$Cu(OH)_2$ film surface in a combinatory study by employing SEM (Fig. 2 and S2†) and GIWAXS measurements (Fig. S3 and S4†), which are discussed below.

In Fig. 2, the top-view SEM images depict the time-dependent growth of the **Cl-DMOF-1**-on-Cu_2bdc_2-on-$Cu(OH)_2$ film structures. Initially, at a growth time of 10 min, small crystallites appear (Fig. 2a), which were determined using GIWAXS measurements to correspond to the weak growth of the **Cl-DMOF-1$_{10min}$** structure (Fig. S3a†). According to the GIWAXS pattern in Fig. S3b,† sharp reflections appear for a growth of 30 min, which are attributed to the formation of the *P4/mmm* phase for the **Cl-DMOF-1$_{30min}$** (a = 10.93 Å, b = 10.93 Å, and c = 9.61 Å).[17,26] Interestingly, (100) reflection shows a shift of Δq = 0.04 nm^{-1} between the out-of-plane (q_{OP} = 5.82 nm^{-1}) and the in-plane direction (q_{IP} = 5.78 nm^{-1}). On the contrary, $(001)_{Cl\text{-}DMOF\text{-}1}$ and $(101)_{Cl\text{-}DMOF\text{-}1}$ reflections remain unaltered, indicating that the (100) plane is distorted. This property is attributed to internal strain[27] within the **Cl-DMOF-1** structures, which becomes more evident at a growth time of 90 min, causing even splitting of $(001)_{Cu_2bdc_2}$ reflection for the Cu_2bdc_2-on-$Cu(OH)_2$ substructure (Fig. S4a,† out-of-plane pattern). Kitagawa and co-workers recently delineated that with a decreasing MOF film thickness, surface effects become more pronounced,[28] in which heteroepitaxial structures can be a display of strain induced by lattice mismatch.[24]

Hence, to understand the impact of internal strain, we performed GIWAXS measurements while rotating the **Cl-DMOF-1$_{90min}$** film sample along the azimuthal angle φ (rotation around the surface normal, see Fig. S5a and b†). The behaviour of the $(100)_{Cl\text{-}DMOF\text{-}1}$ reflection with respect to ϕ in the out-of-plane direction indicates the presence of two crystalline phases. At φ = 0°, the **Cl-DMOF-1$_{90min}$** structure was determined to grow in the *P4/mmm* phase (Fig. S5c and d†), as already encountered for structures grown at shorter times. By rotating the sample to larger φ-angles, a second phase appears that is shifted towards higher q, thus resembling the *I4/mcm* structure (Fig. S5c†). Consequently, the characteristic $(001)_{Cu_2bdc_2}$ reflection of the epitaxial substructure shifts by Δq = 0.03 nm^{-1} towards smaller q in the out-of-plane direction (Fig. S5d†). It must be noted that the Cu_2bdc_2 substructure of the **Cl-DMOF-1$_{90min}$** film was confirmed to comprise a strong azimuthal angle dependence in the in-plane direction (Fig. S5e–g†), as was reported for the non-functionalized DMOF-1 film structure.[22,23] The $(001)_{Cl\text{-}DMOF\text{-}1}$ reflection located at q_{IP} = 6.45 nm^{-1} shows no azimuthal angle dependence in the in-plane direction (Fig. S5b and d†). Based on these findings, we consider the growth of this second *I4/mcm*-like phase a result of relieving the internal strain within the **Cl-DMOF-1** structures that arises mainly from the urge to match the **Cl-DMOF-1** lattice with the lower Cu_2bdc_2-on-$Cu(OH)_2$ structure. Thus, at growth times ≤90 min, strained but heteroepitaxially grown **Cl-DMOF-1**-on-Cu_2bdc_2-on-$Cu(OH)_2$ film systems are obtained. However, a propagation of the growth time leads to non-epitaxially grown **Cl-DMOF-1$_{180min}$** (Fig. S4b†) and **Cl-DMOF-1$_{270min}$** structures (Fig. S4c†). Moreover, the absence of preferred alignment in both in-plane and out-of-plane directions is a characteristic of non-epitaxial and bulk structures.[24]

From SEM micrographs, the evolution of the **Cl-DMOF-1** crystallite growth as a function of time demonstrates the formation of very thin crystallites after 30 min with a size of 1.4 μm in both length and height (Fig. 2b). The **Cl-DMOF-1$_{60min}$** crystallites continue to grow in their width (~0.1 μm; Fig. 2c), which further increases for the **Cl-DMOF-1$_{90min}$** system (~0.3 μm; Fig. 2d). However, prolonged growth of the **Cl-DMOF-1$_{180min}$** system yields crystallites of significantly

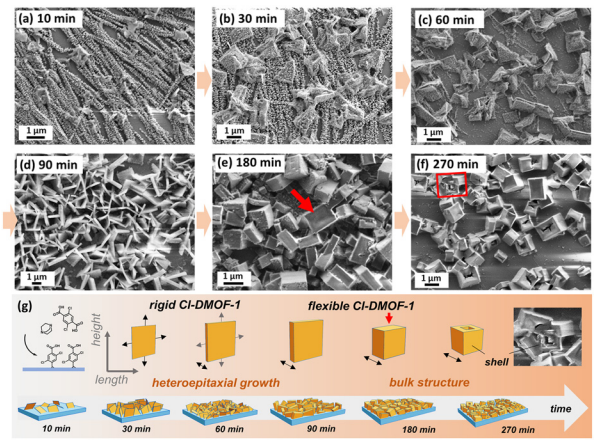

Fig. 2 Representative top-view SEM images of the **Cl-DMOF-1** structure grown on the Cu_2bdc_2-on-$Cu(OH)_2$ substructure for (a) 10 min, (b) 30 min, (c) 60 min, (d) 90 min, (e) 180 min and (f) 270 min. The evolution of crystallite growth is schematically depicted in (g). From left to right: Initially, crystallites preferentially grow in length (10–30 min). After reaching a limiting size, expansion in width begins (60–90 min). Up to 90 min, the crystallites comprise a tetragonal-like shape (width = 0.1 μm), with the length matching the crystallite height. At 180 min, this characteristic shape is lost, whereupon at 270 min, they transform into a cubic shape displaying cracks or bending of the surface (see red arrow), resulting in shell-like crystallites (see the SEM image in the inset).

different shapes, where some crystallite surfaces are strongly bent inward (see the red arrow in Fig. 2e). After 270 min, the crystallite size resembles those of reported bulk crystallites[18] with the difference that most larger crystallites comprise cracks (see Fig. 2f), which are referred to as the result of a long-range strain within the structure.[29] Some of the **Cl-DMOF-1$_{270min}$** crystallites display a hollow core resembling a shell-like structure, which is attributed to the ultimate product of internal stress release (Fig. 2g, see SEM image). The evolution of the **Cl-DMOF-1** crystallite growth is schematically depicted in Fig. 2g, where we classify structures grown shorter than 90 min as heteroepitaxial, while subsequent growth yields bulk-like structures. Based on GIWAXS data, we propose for heteroepitaxial structures (growth time <90 min) that the $(h00)_{\text{Cl-DMOF-1}}$ plane grows epitaxially onto the $(00l)_{Cu_2bdc_2}$ plane with the *a*-axis of the **Cl-DMOF-1** system aligning perpendicular to the substrate. For these structures, the $(00l)_{\text{Cl-DMOF-1}}$ plane orients mainly in the out-of-plane direction, which results in the *c*-axis aligned parallel to the substrate (see Fig. S3a–c†). This alignment was already reported in our earlier study of the oriented DMOF-1 film structure,[22] confirming the isoreticular growth approach for the presented functionalized heteroepitaxial film system. However, this is not the case for bulk-like **Cl-DMOF-1** film structures (180–270 min), which show a sudden change in the alignment of their structure. This property is envisioned by the appearance of the $(00l)_{\text{Cl-DMOF-1}}$ plane in the in-plane direction (≥90 min, Fig. S4a†). We presume that this inversion in alignment mainly arises from the strained ≥180 min structures, resulting in a complete loss of heteroepitaxy accompanied by the sudden change in the shape of the **Cl-DMOF-1** crystallites yielding bulk-like structures (see SEM images in Fig. 2). The growth behaviour of the **Cl-DMOF-1** films was additionally confirmed by infrared spectroscopic measurements. All pristine structures show strong vibrational bands located around 1388 cm^{-1} and 1587 cm^{-1} (Fig. 3 and S6–S8†), corresponding to the symmetric (υ_s) and asymmetric stretching (υ_{as}) of the carboxylic group bonded to the metal nodes, respectively.[22]

We further investigated the structural flexibility of the **Cl-DMOF-1** films. For this, the photo-active guest molecule azobenzene was incorporated within the **Cl-DMOF-1** pores following the vapour-assisted approach (<0.5 molecules per pore, Table S1†).[22] The success of the infiltration process was confirmed by Fourier transform infrared (FT-IR) attenuated total reflectance (ATR) measurements of the respective **Cl-DMOF-1** films. The results show the appearance of the characteristic *trans*-azobenzene vibrational band located around 691 cm^{-1} (see Fig. S6–S8†), which experiences a red shift for structures after prolonged growth (30–180 min, Table S2†). Similarly, a red shift in the υ_s vibrational band was determined, which is attributed to the carboxylate vibrations arising from the **Cl-DMOF-1** structure (Table S2†). This behaviour indicates that the internal strain caused by the heteroepitaxial growth of the **Cl-DMOF-1/AB** structures is directly translated to the infiltrated azobenzene molecule within the pores. In the case of the weakly grown **Cl-DMOF-1/AB$_{10min}$** structure (Fig. S6a†), where the main vibrational bands are attributed to the non-coordinated terephthalic acid linkers (see Fig. S6b†), azobenzene is expected to accumulate on the surface rather than being incorporated within the pores. Hence, this system can serve as a reference because the vibrational band of azobenzene corresponds to its non-strained, pristine *trans*-conformer located at υ_{AB} = 690 cm^{-1} (Fig. S6c†).[30] In comparison, the **Cl-DMOF-1/AB$_{270min}$** system contains azobenzene molecules in a relaxed state (υ_{AB} = 691 cm^{-1}), which is attributed to the loss of epitaxy. Hence, these findings corroborate SEM and GIWAXS measurements; they show that at growth times exceeding 180 min, the internal stress is overcome, which leads to bulk-like, non-epitaxially grown structures.

In the next step, to test the photo-activity of the incorporated azobenzene molecules with respect to the duration of the structural transformation of the **Cl-DMOF-1/AB** systems, we performed ATR measurements combined with two light sources (343 nm and 450 nm; Scheme S2†). The results show that short growth times yield rigid **Cl-DMOF-1/AB** structures where no azobenzene isomerization was possible (Fig. S9a†), while the structures obtained after longer growth times exhibit sufficient flexibility to respond to the azobenzene isomerization process (≥60 min, Fig. S9b†). For the latter films, irradiation by 343 nm prompted the azobenzene within the **Cl-DMOF-1/AB** pores to enter its *cis*-state ($\upsilon_{cis\text{-}AB}$ = 698 cm^{-1}, ON-state), which, after exposure to 450 nm, relaxed fully to its *trans*-conformer ($\upsilon_{trans\text{-}AB}$ = 693 cm^{-1}, OFF-state; Fig. 3b). The results for the **DMOF-1/AB$_{90min}$** show that in the ON state, about 70% of the infiltrated azobenzene molecules are converted to the *cis*-conformer, while 30% of the *trans*-conformer remains (Fig. 3c). This significantly higher abundance of *trans*-azobenzene molecules within the **Cl-DMOF-1/AB$_{90min}$** pores is attributed to the strong stabilization of this conformer owing to the chloro-functionalized MOF

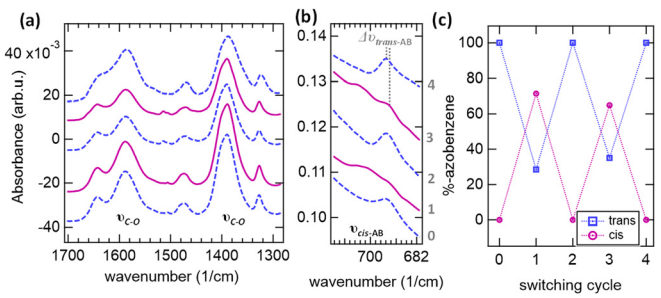

Fig. 3 (a) ATR measurements of the **Cl-DMOF-1/AB$_{90min}$** structure during the photo-switch. (b) Comparison of azobenzene vibrational bands between the excited (purple trace, 343 nm – ON) and the relaxed state (blue trace, 450 nm – OFF) revealed the presence of *cis*-azobenzene ($\upsilon_{cis\text{-}AB}$ = 698 cm^{-1}) in the former and its conversion to the relaxed *trans*-conformer for the latter, with a shift of $\Delta\upsilon_{trans\text{-}AB}$ (ON, OFF) = 1.05 cm^{-1}. (c) Photo-cycling of the system successfully isomerized the azobenzene molecule.

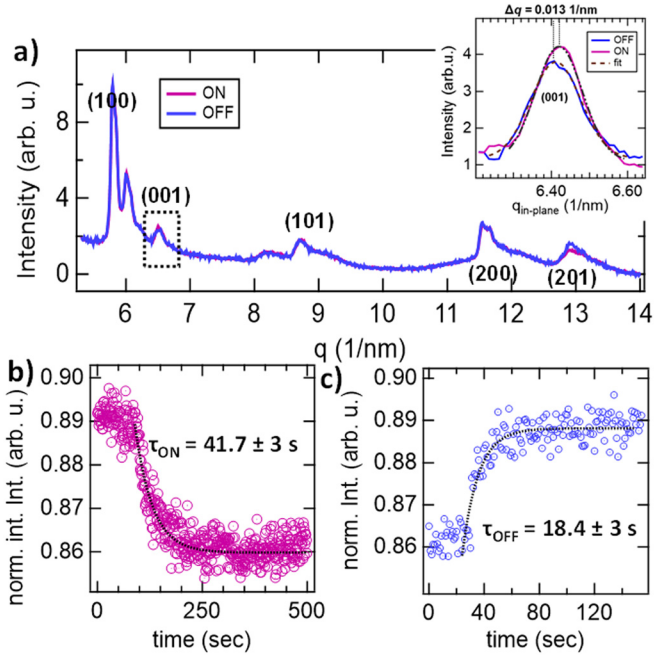

Fig. 4 GIWAXS data for the **Cl-DMOF-1/AB$_{90min}$** structure. (a) Azimuthal integration of the GIWAXS pattern for the switched (ON, purple pattern) and the relaxed **Cl-DMOF-1/AB** film structure (OFF, blue pattern). The change in the intensity of (001) reflection was used to evaluate the switching times (see inset). (b) Considering the change in the normalized integrated (001) intensity, the forward switch (ON, 343 nm) occurred within τ_{ON} = 41.7 ± 3 s, (c) while the back switch (OFF, 450 nm) required τ_{OFF} = 18.4 ± 3 s. Switching constants represent the mean value with corresponding errors derived from experiments conducted by repeating the ON/OFF switch three times.

environment. The relaxed **Cl-DMOF-1/AB$_{90min}$** structure was found to repeatedly allow the azobenzene to enter its *trans*-isomer, exhibiting a shift of $\Delta\upsilon_{cis\text{-}AB}$ = 1.05 cm^{-1} between the ON and OFF states (Fig. 3b).

We further performed time-resolved GIWAXS measurements to investigate the structural transformations induced within the **Cl-DMOF-1/AB$_{90min}$** structure upon photo-excitation. Here, only the **Cl-DMOF-1/AB$_{90min}$** structure was tested to confirm the success of the isomerization process of azobenzene upon photo-stimulation (Fig. 4). This is because azobenzene remains non-responsive at shorter growth times (**Cl-DMOF-1/AB$_{30min}$**; Fig. S9a†), and the bulk-like growth of **Cl-DMOF-1/AB** structures after 180 and 270 minutes produces inhomogeneous films that hinder light penetration, thus impeding their photo-physical characterization.[1] Detailed analysis of the GIWAXS data for the **Cl-DMOF-1/AB$_{90min}$** structure showed that 32% of the crystallites orient preferentially towards the out-of-plane direction (Fig. S10†). This result is comparable to the non-functionalized DMOF-1 film structure, which confirms that an oriented and heteroepitaxial **Cl-DMOF-1** structure is grown, thus allowing the characterization of its photo-switch.[22]

Time-resolved GIWAXS measurements revealed that upon excitation with light of 343 nm, the (001) reflection commenced a shift by Δq = 0.013 nm^{-1}, as determined from fitting results in the in-plane direction (Fig. 4a). This value is in good agreement with findings reported for the non-functionalized DMOF-1 film system.[22] Hence, the **Cl-DMOF-1/AB$_{90min}$** structure shrinks when azobenzene enters its *cis*-conformer, which is reversed by the light of 450 nm upon relaxation to its *trans*-conformer (Fig. 4b and c). This finding strongly supports the successful isoreticular design strategy as the structural response for the **Cl-DMOF-1** is channelled similarly to the DMOF-1 structure.[22] From the temporal evolution of the intensity for the (001) reflection under continuous illumination with the respective light sources, the switching constants were deduced for the ON state (343 nm, Fig. 4b) and the OFF state (450 nm, Fig. 4c). GIWAXS measurements showed that the structural response for the ON state was reached after τ_{ON} = 41.7 ± 3 s (343 nm@130 mW cm^{-2}), which was reversed within τ_{OFF} = 18.4 ± 3 s (Fig. 4b and c; 450 nm@17.2 mW cm^{-2}). In comparison, we reported for the non-functionalized DMOF-1 film structure that the entire switch required 15 s (343 nm@95 mW cm^{-2}, 450 nm@17.2 mW cm^{-2}),[22] therefore rendering the **Cl-DMOF-1/AB$_{90min}$** film system to respond significantly slower at similar irradiances (see Table S3† for comparison of the two film systems). This finding is reasonable because chloro-functionalized switchable bulk structures are known to experience a certain loss in flexibility,[16] as indicated by the lack of gate-opening behaviour in bulk **Cl-DMOF-1** during N_2 sorption experiments, while the DMOF-1 showed a subtle step in the adsorption branch P/P_0 = 0.003 (Fig. S13†).

In conclusion, we herein prepared Zn-based MOF films using chlorinated terephthalic acid and dabco as ligands, yielding 3D-oriented MOF crystals infiltrated with photo-responsive azobenzene. Upon UV irradiation, we measured orthogonal stimulation. The chloro-functionality imparts rigidity to the oriented MOF film, leading to a strongly decelerated structural photo-response. Depending on the synthesis conditions, different photo-responsive behaviours were observed: films prepared with short reaction times (10–60 min) showed entirely rigid frameworks, while prolonged growth of the MOF crystals (90–270 min) yielded more flexible structures. Moreover, the azobenzene molecules in the MOF pores can be repeatedly isomerized when triggered by light opening possibilities for their application as mechanical storage systems.[10,12,15,17]

Conflicts of interest

There are no conflicts to declare.

Acknowledgements

We thank Ing. Andrea Radeticchio and Dr Barbara Sartori for experimental and technical support. S. K. would like to acknowledge CERIC-ERIC for the postdoctoral position granted through its internal project 'INCITE'. The authors also acknowledge the CERIC-ERIC Consortium for access to

the Austrian SAXS beamline and SISSI beamline at ELETTRA through proposal No. 20212195 and 20222149.

Notes and references

1 R. Haldar, L. Heinke and C. Wöll, *Adv. Mater.*, 2020, **32**, e1905227.
2 J. Liu and C. Wöll, *Chem. Soc. Rev.*, 2017, **46**, 5730–5770.
3 A. H. Assen, O. Yassine, O. Shekhah, M. Eddaoudi and K. N. Salama, *ACS Sens.*, 2017, **2**, 1294–1301.
4 A. B. Kanj, J. Bürck, S. Grosjean, S. Bräse and L. Heinke, *Chem. Commun.*, 2019, **55**, 8776–8779.
5 J. Della Rocca, D. Liu and W. Lin, *Acc. Chem. Res.*, 2011, **44**, 957–968.
6 J. Gandara-Loe, B. E. Souza, A. Missyul, G. Giraldo, J.-C. Tan and J. Silvestre-Albero, *ACS Appl. Mater. Interfaces*, 2020, **12**, 30189–30197.
7 A. Bui, S. G. Guillen, A. Sua, T. C. Nguyen, A. Ruiz, L. Carachure, M. D. R. Weber, A. Cortez and F. Tian, *Colloids Surf.*, 2022, **650**, 129611.
8 H. B. Wu and X. W. Lou, *Sci. Adv.*, 2017, **3**, eaap9252.
9 M. Linares-Moreau, L. A. Brandner, M. de Velásquez-Hernández, J. Fonseca, Y. Benseghir, J. M. Chin, D. Maspoch, C. Doonan and P. Falcaro, *Adv. Mater.*, 2023, **36**, 2309645.
10 J. Wieme, S. M. Rogge, P. G. Yot, L. Vanduyfhuys, S.-K. Lee, J.-S. Chang, M. Waroquier, G. Maurin and V. Van Speybroeck, *J. Mater. Chem. A*, 2019, **7**, 22663–22674.
11 Q. Huang and C. Wu, *Mater. Today Sustain.*, 2022, **18**, 100149.
12 F. Bigdeli, C. T. Lollar, A. Morsali and H.-C. Zhou, *Angew. Chem., Int. Ed.*, 2020, **59**, 4652–4669.
13 N. Yanai, T. Uemura, M. Inoue, R. Matsuda, T. Fukushima, M. Tsujimoto, S. Isoda and S. Kitagawa, *J. Am. Chem. Soc.*, 2012, **134**, 4501–4504.
14 R. Lyndon, K. Konstas, B. P. Ladewig, P. D. Southon, C. J. Kepert and M. R. Hill, *Angew. Chem., Int. Ed.*, 2013, **52**, 3695–3698.
15 S. B. Peh, A. Karmakar and D. Zhao, *Trends Chem.*, 2020, **2**, 199–213.
16 T. Devic, P. Horcajada, C. Serre, F. Salles, G. Maurin, B. Moulin, D. Heurtaux, G. Clet, A. Vimont, J.-M. Grenèche, B. Le Ouay, F. Moreau, E. Magnier, Y. Filinchuk, J. Marrot, J.-C. Lavalley, M. Daturi and G. Férey, *J. Am. Chem. Soc.*, 2010, **132**, 1127–1136.
17 K. Griffiths, N. R. Halcovitch and J. M. Griffin, *Chem. Mater.*, 2020, **32**, 9925–9936.
18 M. Xie, N. Prasetya and B. P. Ladewig, *Inorg. Chem. Commun.*, 2019, **108**, 107512.
19 H. Hahm, K. Yoo, H. Ha and M. Kim, *Inorg. Chem.*, 2016, **55**, 7576–7581.
20 S. Henke, A. Schneemann, A. Wütscher and R. A. Fischer, *J. Am. Chem. Soc.*, 2012, **134**, 9464–9474.
21 N. C. Burtch and K. S. Walton, *Acc. Chem. Res.*, 2015, **48**, 2850–2857.
22 S. Klokic, D. Naumenko, B. Marmiroli, F. Carraro, M. Linares-Moreau, S. D. Zilio, G. Birarda, R. Kargl, P. Falcaro and H. Amenitsch, *Chem. Sci.*, 2022, **13**, 11869–11877.
23 M. Linares-Moreau, L. A. Brandner, T. Kamencek, S. Klokic, F. Carraro, K. Okada, M. Takahashi, E. Zojer, C. J. Doonan and P. Falcaro, *Adv. Mater. Interfaces*, 2021, **8**, 2101039.
24 P. Falcaro, K. Okada, T. Hara, K. Ikigaki, Y. Tokudome, A. W. Thornton, A. J. Hill, T. Williams, C. Doonan and M. Takahashi, *Nat. Mater.*, 2017, **16**, 342–348.
25 N. Novendra, J. M. Marrett, A. D. Katsenis, H. M. Titi, M. Arhangelskis, T. Friščić and A. Navrotsky, *J. Am. Chem. Soc.*, 2020, **142**, 21720–21729.
26 D. N. Dybtsev, H. Chun and K. Kim, *Angew. Chem., Int. Ed.*, 2004, **43**, 5033–5036.
27 T. O. Erinosho, D. M. Collins, A. J. Wilkinson, R. I. Todd and F. Dunne, *Int. J. Plast.*, 2016, **83**, 1–18.
28 T. Haraguchi, K. Otsubo and H. Kitagawa, *Eur. J. Inorg. Chem.*, 2018, 1697–1706.
29 H. Aggarwal, P. M. Bhatt, C. X. Bezuidenhout and L. J. Barbour, *J. Am. Chem. Soc.*, 2014, **136**, 3776–3779.
30 J. D. Webb, H. H. Neidlinger and J. S. Connolly, *Polym. Chem.*, 1986, **7**, 503–515.

